IEEE Access
Multidisciplinary ⋮ Rapid Review ⋮ Open Access Journal

Received May 10, 2020, accepted May 13, 2020, date of publication May 18, 2020, date of current version June 1, 2020.

Digital Object Identifier 10.1109/ACCESS.2020.2995298

Grid-Forming Power Converters Tuned Through Artificial Intelligence to Damp Subsynchronous Interactions in Electrical Grids

GREGORY N. BALTAS[1], (Student Member, IEEE), NGOC BAO LAI[1,2], (Student Member, IEEE), LEONARDO MARIN[2], (Student Member, IEEE), ANDRÉS TARRASÓ[2], (Student Member, IEEE), AND PEDRO RODRIGUEZ[1,2], (Fellow, IEEE)

[1]Loyola Institute of Science and Technology (Loyola.TECH), Universidad Loyola Andalucía, 41704 Seville, Spain
[2]Renewable Electrical Energy Systems (SEER), Technical University of Catalonia, 08222 Terrassa, Spain

Corresponding authors: Gregory N. Baltas (ngbaltas@uloyola.es) and Ngoc Bao Lai (nblai@uloyola.es)

This work was supported in part by the European Commission under Project FLEXITRANSTORE—-H2020-LCE-2016-2017-SGS-774407, and in part by the Spanish Ministry of Science under Project ENE2017-88889-C2-1-R.

ABSTRACT The integration of non-synchronous generation units and energy storage through power electronics is introducing new challenges in power system dynamics. Specifically, the rotor angle stability has been identified as one of the major obstacle with regards to power electronics dominated power systems. To date, conventional power system stabilizer (PSS) devices are used for damping electromechanical oscillations, which are only tuned sporadically leading to significant deterioration in performance against the ever-changing operating conditions. In this paper, an intelligent power oscillation damper (iPOD) is proposed for grid-forming converters to attenuate electromechanical inter-area power oscillation. In particular, the iPOD is applied to a synchronous power controller (SPC) based grid-forming power converter to increases gain of the active power control loop at the oscillatory frequency. Predictions regarding the mode frequency, corresponding to the current operating points, are given by an artificial intelligence ensemble model called Random Forests. The performance of the proposed controller is verified using the two area system considering symmetrical fault for random operating points. In addition, a comparison with PSS installed in each generator reveals the individual contribution with respect to the inter-area mode damping.

INDEX TERMS Artificial intelligence, ensemble modelling, inter-area power oscillation, random forests, synchronous power controller.

I. INTRODUCTION

Renewable-based Energy Systems (RES) and Energy Storage Systems (ESS) are widely adopted to reduce green house gas emissions and improve efficiency. These systems, due to their incompatibility with synchronous frequency (50/60 Hz), require power electronic devices to act as an intermediate before connection with the rest of the network is possible. Consequently, as the presence of power electronics increases, the power system dynamics are affected introducing new challenges regarding power system stability [1]. In fact, ENTSO-E has identified the angular stability of power systems as one of the key challenges related to High Penetration of Power Electronic Interfaced Power Sources (HPoPEIPS) [2].

The associate editor coordinating the review of this manuscript and approving it for publication was Xiaorong Xie.

Conventionally, the PSS has been used to damp low frequency oscillations in a system by regulating the synchronous generator's excitation voltage.Among the standardized PSS schemes, the classical PSS1 controller consists of three main blocks: gain, washout filter and phase compensation. Considering inter-area modes, the time constant of the washout filter needs to be carefully chosen, since it captures the low frequency oscillations [3]. The PSS1 uses a single input signal, typically the speed deviation $\Delta\omega$. More sophisticated designs are the PSS2B and PSS4B controllers. In PSS2B, speed transducers are added to improve reactive power modulation during mechanical power changes and eliminate torsional forces that can harm the generator shaft. PSS4B builds on top of the PSS2B by incorporating low, intermediate and high frequency bands to broaden the range of targeted modes [4].

One major limitation of the PSS is the high number of parameters that need to be tuned for attenuating system

oscillations [5]. For instance, a typical PSS has 8 parameters: gain, time constant of wash out filter, and four constants for lead-lag compensator. These parameters usually are tuned at commissioning of the power plant and remain fixed despite the changes of operating conditions [6]. There is an open discussion in the literature on possible methods for adaptive PSS and optimal tuning [3]. This becomes even more relevant now, as power electronics can alter the oscillatory profile of a given system, changing or creating new modes.

Currently, the number of synchronous generators is slowly phased out [7] and as a result so will the number of PSS. Yet, power electronic interfaced generation units can provide a fast response to the grid and assist the system in maintaining its stability in case of a disturbance [8]. Such grid friendly response can be produced by means of the currently well-known grid-forming power converters. In general, the control system of a grid-forming converter can either be based on droop [9] or on virtual synchronous machine (VSM) [10]. In the former case, the contribution of the power converter is usually limited to primary frequency and voltage regulation. To add grid-supporting functionalities, e.g. inertia emulation and power oscillation damping, the VSM implementation can be adopted in the grid-forming power converter [11].

Among the various VSM strategies, reported in the literature, the Synchronous Power Controller (SPC) has been widely used mainly due its simple yet effective control structure [12]. By employing the SPC, power converters can provide virtual damping and synthetic inertia to the grid, increasing its dynamic flexibility to improve local and inter-area stability [13], [14]. In fact, the SPC with multiple power loop controllers (PLC) has been presented in [15]. By combining a band-pass filter with a modified swing equation, the inter-area oscillations at a predefined frequency can be attenuated. However, to ensure the system in [15] works effectively, the center frequency of its band-pass filter has to be tuned properly to match the frequency of the inter-area oscillation mode, which is usually not accessible due to the dynamic behavior of the power system.

Recently, data-driven methods based on artificial intelligence (AI) are studied for accurately and efficiently determining the state of the power system in real time and thereby avoid instability [16]. Specifically, the relationship between system variables and stability indexes can be modeled to predict the post-fault state of the system. For instance, an ensemble approach based on extreme learning machines is adopted in [17] to predict stability after a disturbance, while a recurrent neural network with long short term memory (LSTM) cells is trained in [18] for the same task considering time dependencies in the data. Furthermore, prediction of damping state (i.e. well or poorly damped) is proposed by [19] using decision trees and by [20] using neural networks.

Driven from the above, this paper presents an intelligent Power Oscillation Damper (iPOD) that enables the SPC to adapt for maximum -oscillatory- mode attenuation. The iPOD is based on an ensemble AI predictor called Random Forests (RF), which is trained to predict the real and imaginary components of the targeted mode of oscillation as it moves according to the current operating conditions. The main contribution of the system, presented in the following, is a novel control scheme that incorporates intelligence by exploiting the ability of AI to predict the characteristic values of an oscillatory mode in real time and uses this information to adaptively tune a dedicated loop of the SPC to damp oscillations and enhance the system stability i.e. iPOD. In this work, special focus is put on describing all the steps for developing the AI models in detail. The proposed approach is verified under a symmetrical fault for random operating points as well as against conventional PSS devices using the well-known two area system described in [21]. The AI predictor is trained for tracking the inter-area mode between the two areas, however the same principles can be applied to develop multiple AI predictors to predict more than one inter-area modes.

The remainder of this paper is structured as follows. Section II provides a detail description regarding the test case. Section III presents the proposed AI-based adaptive SPC model. Section IV analyse the results and Section V discusses the conclusions.

II. TEST CASE

A popular power system to analyse the behavior of an inter-area mode is the two-area system [21], depicted in Fig. 1. The system consists of two areas with one load (L07, L09), one shunt capacitor (C7, C9) and two generators (G1-G2, G3-G4), respectively. Each generator is equipped with IEEE Type AC4A Excitation System (AVR), steam turbine governors (GOV) and PSS type 1. These areas are connected through a weak tie-line where 400MW are flowing from Area 1 to Area 2. Modal analysis reveals two local modes with frequencies of 1.05Hz and 1.08Hz in Area 1 and Area2, respectively, as well as an inter-area mode with frequency of approximately 0.55Hz.

The specific design of this system not only allows for studying the behaviour of electromechanical oscillations between two areas, but also on demonstrating the effectiveness of control methods (such as the iPOD) for attenuating them. To demonstrate the impact of the iPOD, a virtual-synchronous generation unit equiped with an SPC is connected at bus 7, through two step-up transformers. The rated apparent power of the aforementioned unit is 100MVA, equal

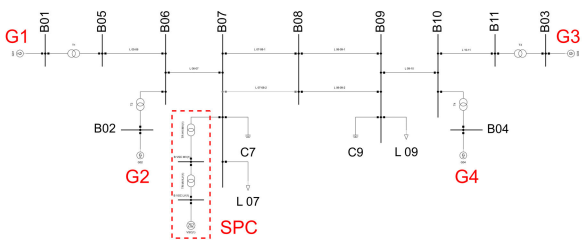

FIGURE 1. Modified two area system.

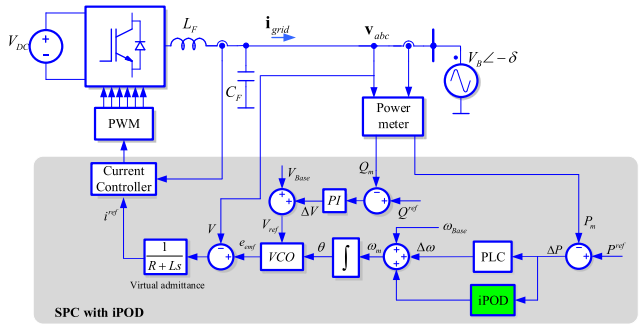

FIGURE 2. Block diagram of RF-SPC.

to 3% of the total apparent power of the four synchronous generators together.

III. iPOD FOR GRID-FORMING CONVERTERS

A. CONTROL STRUCTURE

For mitigating inter-area oscillations, a conventional SPC is equipped with an iPOD as shown in Fig. 2. Generally, the SPC consists of four main control blocks, namely, the current controller, the virtual admittance, the reactive controller, and the PLC. In the SPC, the reference for the current control loop is generated by means of a virtual admittance whose transfer function is

$$Y(s) = \frac{1}{Ls + R} \tag{1}$$

where R and L are the virtual resistance and the virtual inductance, respectively. As shown in Fig. 2, the virtual electromotive force e_{emf} is generated by combining the outputs of the active and reactive control loops through a voltage-controlled oscillator (VCO) as

$$e_{emf} = V_{ref} sin(\theta). \tag{2}$$

In (2), the magnitude of the electromotive force is regulated through the reactive power controller as follows:

$$V_{ref} = V_{Base} + k_p(Q^{ref} - Q_m) + k_i \int (Q^{ref} - Q_m)dt \tag{3}$$

where k_p and k_i are the proportional and integral gains of the reactive power controller, and V_{based} is the nominal voltage. Likewise, the phase angle θ used in (2) is produced by the active power loop controller (PLC). In this implementation, although any other controller structure could be used [8], the PLC is implemented through the conventional swing equation whose transfer function is

$$G_{PLC}(s) = \frac{1}{2Hs + D} \tag{4}$$

where H and D are the inertia constant and the damping coefficient respectively, while ω_{base} is the grid nominal frequency, which acts as a feed-forward term to improve the dynamic performance of the SPC.

Aiming to increase damping to inter-area oscillation modes, the PLC is incorporated with the proposed iPOD as

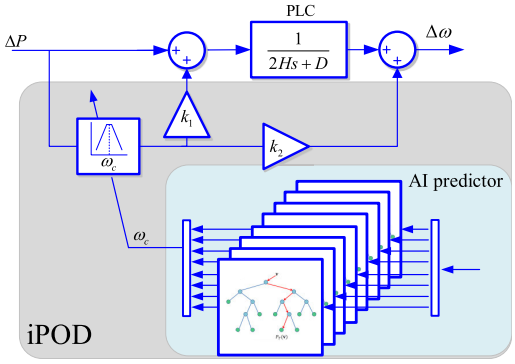

FIGURE 3. Intelligent power oscillation damper (iPOD).

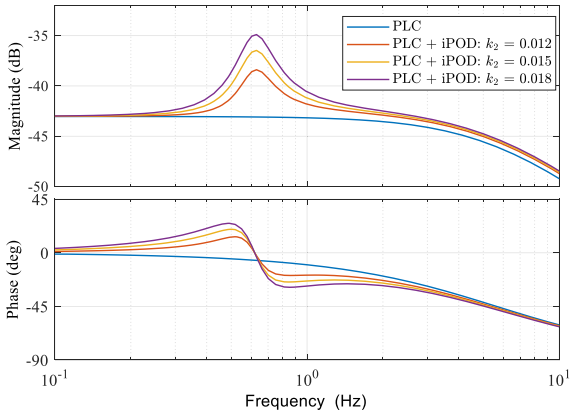

FIGURE 4. Frequency response of the conventional PLC and the proposed PLC.

shown in Fig. 3. Essentially, the iPOD includes two proportional gains k_1 and k_2, and a second-order band-pass filter. The gain k_1 is set to -1 for removing the targeted frequency component from the signal before acted on the PLC, whereas k_2 defines the damping factor provided by the iPOD at the specified frequency. The reason behind the choice of a band-pass filter is that the frequency of the oscillation is considered to be a known parameter. Indeed, the oscillation frequency is predicted by the AI predictor which will be explained in the following subsections. The transfer function of the band-pass filter can be given as

$$G_{BPF}(s) = \frac{Bs}{s^2 + Bs + \omega_c^2} \tag{5}$$

where ω_c is centre frequency and B is passing band. From (4) and (5), the augmented transfer function of the active power controller can be derived as follows:

$$\begin{aligned} G_p(s) &= G_{PLC}(s) + G_{BPF}(s)\,[k_1 G_{PLC}(s) + k_2] \\ &= G_{PLC}(s) + G_{BPF}(s) G_{ll}(s) \\ &= \frac{(2BHk_2 + 1)s^2 + (B + Bk_1 + BD\,k_2)s + \omega_c^2}{2Hs^3 + (D + 2BH)s^2 + (2H\omega_c^2 + BD)s + D\omega_c^2} \end{aligned} \tag{6}$$

From (6), the combined frequency response of the PLC and the iPOD is obtained, as depicted in Fig. 4 for different

values of gain k_2. As shown, the iPOD adds a significant amplification to the active power control loop at the tuned frequency. Such a high gain implies that the proposed PLC with iPOD control structure can provide higher damping to low-frequency inter-area oscillation.

It is worth noting that the augmented transfer function (6) has two parts. While the first term is conventional PLC, the second term reflects added effects of the iPOD. In fact, the second term can be rewritten in a form of a lead-lag compensator as follows:

$$G_{ll}(s) = \frac{2k_2Hs + (k_1 + k_2D)}{2Hs + D}. \tag{7}$$

Equation (7) reveals that the two gains k_1 and k_2 make it possible to adjust not only gain but also phase lag of the active power control loop at the specified frequency. In practice, the inter-area modes depends on the operating condition of the electrical grid. Therefore, in order to predict the oscillation modes in real-time, the AI-based algorithm called Random Forest is employed.

B. ENSEMBLE AI PREDICTOR

The structure of the proposed iPOD requires up to date information regarding the targeted mode's frequency to provide additional damping. Therefore, its imperative to develop a model that will be able to relate the systems operating condition to the specific movement of the targeted mode. Although this can be a challenging task, following a purely mathematical approach, data-driven methods based on AI and machine learning are able to approximate this relationship without any knowledge about the inner mechanics of the system.

Among the plethora of machine learning models, such as the neural network in [22] to improve damping control for Static Synchronous Series Compensator, the decision tree (DT) stands out due to its robustness against feature scales or types, meaning that it is possible to process patterns with metric and non-metric data at the same time [23]. In addition, the decision making process of the DT is highly interpretable, e.g. as in Fig. 5, and is able to remove redundant system variables, thus performing an intrinsic feature selection.

The basic principle of DTs is to classify patterns based on a series of ''questions'', where the given answer determines the next ''question'' being asked and so on. This top-down process can be displayed in the form of a tree, consisting of nodes and branches as illustrated in Fig. 5. The process begins at the root node and it ends at the leaf nodes, where the process stops. The ''question'', more formally known as the split criterion of the node, resembles an ''if-then-else'' statement that describes a specific rule. For instance, the root node of the DT depicted in Fig. 5, reveals a threshold value for the Voltage magnitude (V_m) at bus 09. Depending on the answer the subsequent question can be either about the Power Factor (PF) at bus 10 or at bus 9, as in (8). This rule based approach is the core of the high level of transparency, which

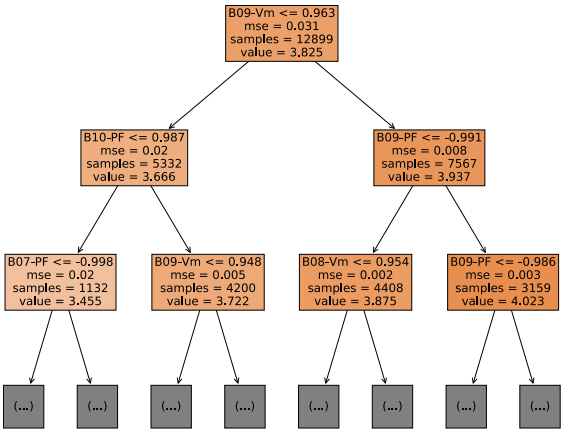

FIGURE 5. Feature space segmentation of a regression tree.

is not found in other machine learning models.

$$V_m^{B09} \leq 0.963 \Rightarrow \begin{cases} Yes & \Rightarrow PF^{B09} \leq -0.991 \\ No & \Rightarrow PF^{B10} \leq 0.987 \end{cases} \tag{8}$$

Generally, the purpose of the splitting criterion is to divide the feature space into as pure as possible sub-spaces. Hence, for every candidate split criterion the resulted impurity is calculated as the mean squared error, see (9), between the true value $y^{(i)}$ and predicted value $\hat{y}_t$ for patterns in subset S_t averaged over all training patterns N_t at node t. The predicted value at node t is calculated according to (10).

$$I(t) = \frac{1}{N_t} \sum_{i \in S_t} (y^{(i)} - \hat{y}_t)^2, \tag{9}$$

$$\hat{y}_t = \frac{1}{N_t} \sum_{i \in S_t} (y^{(i)}) \tag{10}$$

The efficiency of a split criterion is further validated by calculating the drop of impurity at the ancestor nodes, as in (11). Here, t_Y and t_N are the two ancestor nodes corresponding to the *Yes* and *No* branches, while N_{tY}/N_t and N_{tN}/N_t are the portion of samples at each of the these two nodes. Ultimately, at each node, the final splitting rule is chosen to be the one that reduces the impurity at the ancestor nodes the most [24].

$$\Delta I(t) = I(t) - \frac{N_{tY}}{N_t} I(t_Y) - \frac{N_{tN}}{N_t} I(t_N), \tag{11}$$

Despite their straightforward interpretation and intuitiveness, DTs tend to overfit the data demonstrating poor generalization. Moreover, errors propagate from higher level nodes towards lower level nodes [24] resulting in a different DT if changes to the training data occur.

To overcome the avove limitations, an ensemble AI model called Random Forest (RF) is adopted, which integrates multiple DTs into a single predictor, as in Fig. 6. The individual DTs are trained, based on the principle describe above, for the same task but separately from each other, using random subsets of patterns (i.e. system snapshots) and/or features (i.e. system variables). The random sampling is widely known as

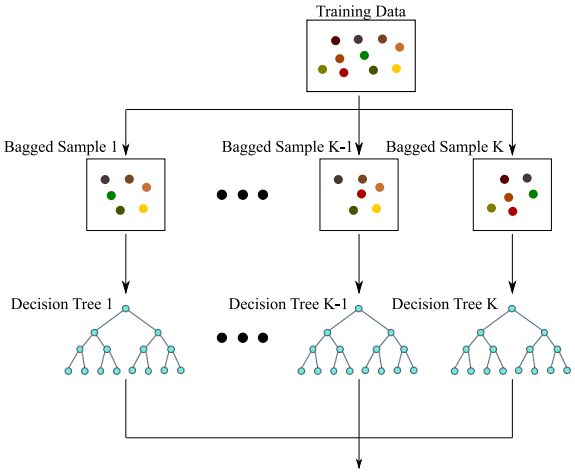

FIGURE 6. Bagging ensemble - random forests.

bootstrap aggregation (or bagging for short [23]) when the subsets are not unique. The ensemble paradigm demonstrates higher performance both in terms of accuracy and generalization: a direct consequence of the diversity promoted by the randomness of the different subsets that are used for developing each of the individual prediction models.

Frequently, the final output of the ensemble is given through a majority voting scheme [25] or by averaging the probabilistic prediction (i.e. soft voting). Nevertheless, the core of RF are the individual DTs where the development process is the same, albeit the variations of the feature-pattern space.

C. ENSEMBLE AI PREDICTOR TRAINING AND TUNING

1) DATABASE DESCRIPTION

To generate a sufficient amount of measurements, an automated simulation process is designed to parse through a wide range of probable operating scenarios, and to store the variables of interest. In other words, this automated process will formulate a database $D \in \mathbb{R}^{M\times N}$, where $M \in \mathbb{Z}^{+}$ is the total number of patterns and $N \in \mathbb{Z}^{+}$ is the total number of features.

DigSilent's PowerFactory is the selected platform to run the simulations and Python 3.7 for executing *Algorithm 1*. The loading of the system (line 3 of *Algorithm 1*) is chosen from (12), where $r_{1,2} \sim U(0,1)$ are random coefficients drawn from a uniform distribution between the open set 0 and 1, μ is the distribution mean and σ is the standard deviation. The processing time on a machine with 20 processors and a single Powerfactory licence requires around 50 minutes per 1000 simulations. Our final dataset consists of about 22000 patterns and 122 features, i.e. $D \in \mathbb{R}^{22000\times 122}$. A summary of the system variables constituting our feature vector can be found in Table 1.

$$\beta = \mu + \sigma\sqrt{-2\log(r_1)}\cos(2\pi r_2) \tag{12}$$

For each pattern in the dataset there exists a set of eigenvalues that corresponds to a random operating point. From the set of eigenvalues the most dominant mode is extracted, in this case the inter-are mode. Hence, each pattern is labeled with the target variable comprised of the real and imaginary component i.e. $\mathbf{y} \in \mathbb{R}^{22000\times 2}$.

The behaviour of dominant inter-area mode for the random operating points is revealed in Fig. 7. From the figure it becomes apparent that there are many instances were the dominant inter-area mode moved to the, unstable, right hand side of the real axis. In addition, the frequency of the dominant inter-area mode varies significantly, as the conditions change, from 0.45Hz up to 0.76Hz. Interestingly, from Fig. 8 it appears to exist a relationship between voltage magnitude and voltage angle that can be used by the RF to map system variables to the inter-area mode. For example, almost every voltage magnitude that corresponds to the unstable inter-area mode is less than 1 p.u. Similar patterns can be seen in other locations of the system not presented here for brevity.

Algorithm 1 Generate Data-Set

```
1: input M
2: while m < M do
3:    Randomly Set P and Q
4:    Calculate Power Flow
5:    if Success then
6:       Perform Modal Analysis
7:       Store Results
8:       m ← m + 1
9:    end if
10: end while
```

TABLE 1. Monitored system variables.

Element	Variable	Units
Bus	Voltage Magnitude	p.u.
	Voltage Angle	deg
Generator	Loading	%
	Current Magnitude	p.u.
	Current Angle	deg
	Loading	%
Transmission Line	Losses	kW
	Active Power	MW
	Reactive Power	Mvar
	Power Factor	

2) PREPROCESSING

The simulated environment assumes full observability of the system, that is, measurements of system variables are recorded in every location of the system. However, in reality this can be costly and impractical. In addition correlated features can impair the ability of a prediction model to make accurate predictions. Therefore, several methods are used for reducing the size of the feature vector to include only relevant and uncorrelated features. In general, the objective of data preprocessing is mainly two-fold; to improve the accuracy of the model and its training speed [26].

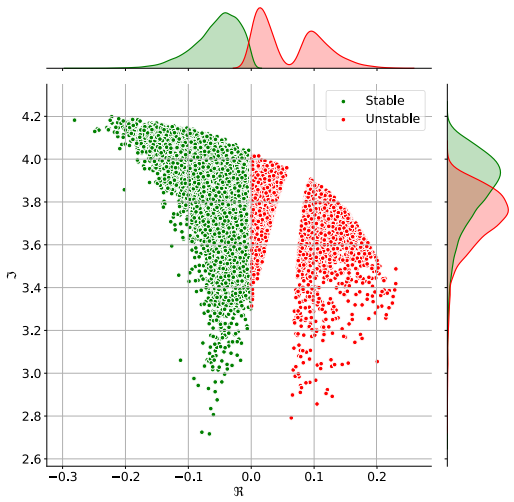

FIGURE 7. Modal analysis results of *algorithm 1*.

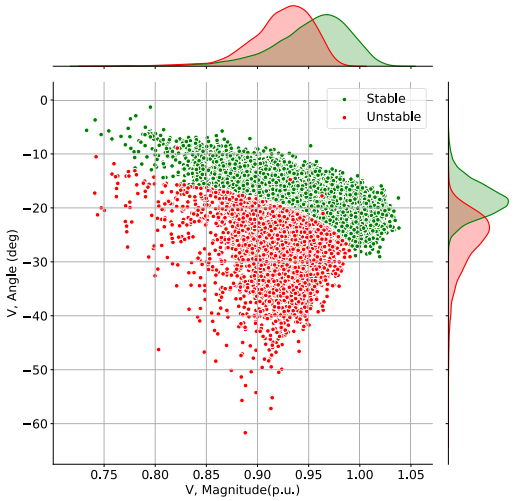

FIGURE 8. Kernel density estimate of voltage magnitude in bus 08 for random operating conditions.

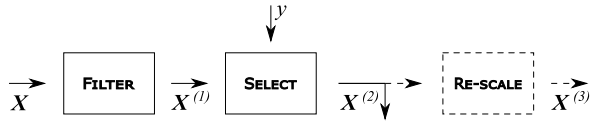

FIGURE 9. Data preprocessing workflow.

The typical workflow followed for processing a dataset consists of three steps: *filter*, *select* and *re-scale* as in Fig. 9. However, due to the robustness of DTs to features of different scale and type last step can be omitted, as indicated by the dashed lines in Fig. 9.

The highly correlated features are filtered out by using a minimum acceptance threshold and Pearson's correlation coefficient, as in (13), where $\{j, p \in [1, \ldots, N] \mid j \neq p\}$ are feature indexes while the bar above the variable denotes the sample mean. The uncorrelated features comprising the feature vector reduced from 122 to just 36 features.

The inherent ability of DTs and RFs to perform feature elimination is exploited to analyse the individual contribution of each feature in the prediction process. Typically, greedy search algorithms like the Sequential Feature Selection (SFS) are preferred as they require less time and computational resources to eliminate features [26]. Fortunately, the size of the feature vector in hand allows the implementation of exhaustive search algorithms such as the Recursive Feature Elimination (REF), which guarantee optimal feature elimination. In this study, the REF algorithm is used alongside the RFs to decrease the size of the feautere vector even further to only 22.

$$r = \frac{\sum_{i=1}^{M}(x_{i,j} - \overline{x_j})(x_{i,p} - \overline{x_p})}{\sqrt{\sum_{i=1}^{M}(x_{i,j} - \overline{x_j})^2 (x_{i,p} - \overline{x_p})^2}} \tag{13}$$

The RFs are trained in python 3.7 using the *scikit-learn* package [27]. Although it is possible to predict both real and imaginary parts of eigenvalues with a single RF, here it is preferred to train a separate RF for each component. Therefore, if performance drops for one of the two target variables, the problematic model can be still retrained without losing the predictions for the other variable.

The optimal parameters, valid for both RF models, are estimated using grid search and summarized in Table 2. Notice that three out of five parameters refer to the development of the individual DT. Specifically, the minimum patterns per split define a lower bound to the number of patterns needed to make a split, the maximum features define the number of features to be considered for the split criterion at each node, while the maximum depth sets an upper bound to the DT growth. Finally, the Bootstrap implies feature and pattern sampling selection is done with replacement. The RF is evaluated using a 10-fold cross validation, recording both the R2 score, in (14) and Mean Absolute Error (MAE), in (15). The former measures how well the features explain the target variable with values ranging from 0 (worse) to 1 (best).

$$R^2(y, \hat{y}) = 1 - \frac{\sum_{i=1}^{n}(y_i - \hat{y}_i)^2}{\sum_{i=1}^{n}(y_i - \bar{y})^2} \tag{14}$$

$$\mathrm{MAE}(y, \hat{y}) = \frac{1}{n_{\text{patterns}}} \sum_{i=0}^{n_{\text{patterns}}-1} \left| y_i - \hat{y}_i \right|. \tag{15}$$

3) PERFORMANCE ANALYSIS

Learning curves are showing the performance of a machine learning model as a function of the training set's size.

TABLE 2. Random forests parameters.

Parameter	Value
Decision Trees	1000
Bootstrap	*yes*
Minimum Patterns/Split	5
Maximum Features	$log_2(22)$
Maximum Depth	80

Particularly, Fig. 10 depicts the learning curve of the RF model developed to predict the $\Im\{\lambda\}$ component of inter-area mode. The figure clearly shows that after 8000 training patterns there is no significant gain in the performance of the RF model. Hence, by using fewer training patterns we can limit the time spent for fitting the model to just $30s$. Furthermore, the cross-validation score seems to converge to a certain value indicating that further addition of training data cannot improve the model. Similar behaviour can be viewed for the corresponding model of the $\Re\{\lambda\}$ component not shown here due to space limitations.

In addition to the metrics described in the previous section, both training and testing CPU processing times are considered. The cross validated accuracy and speed of $\Re$-RF and $\Im$-RF are listed in Table 3. The tables prove the high accuracy of RF to predict both the real and imaginary values of the inter-area mode. The error of the $\Re$-RF is slight lower than the one calculated for $\Im$-RF however the difference is quite small. On average a single RF model needs approximately $50s$ for training and $0.7s$ on a high performance computer using 32 CPUs.

TABLE 3. Random forests performance.

	$\Re\{\lambda\}$		$\Im\{\lambda\}$	
Metric	Train	Test	Train	Test
R2	0.9995	0.9976	0.9994	0.9977
MAE	0.0002	0.0004	0.0004	0.0008
CPU	$49.93s$	$0.65s$	$46.15s$	$0.62s$

Overall, both RFs demonstrate high accuracy on predicting the inter-area mode using only 22 system variables. Concretely, RFs can provide accurate information about the inter-area mode such as damping, frequency and damping ratio. Although the iPOD is designed for tracking and attenuating the inter-area mode between the two areas, the same principles can be applied to develop the iPOD for more than one inter-area modes. This implies that the iPOD will be modified by integrating multiple AI predictors (or a single multi-output AI predictor) and multiple band pass filters [15] as dictated by the number of inter-area modes in the system. Multiple inter-area mode attenuation is however, out of the scope of this paper. The next step is to verify that this information allows the iPOD to realize mode attenuation and enhance system stability.

IV. VERIFICATION

The intelligence of the iPOD scheme, proposed in this paper, for the SPC is based on the premises that a machine learning model, like RF, can predict in real time the dominant mode real and imaginary components. Specifically, the SPC can utilize the prediction about the mode's frequency to re-tune the iPOD band-pass filter to adapt in the new operating conditions. The gains of the iPOD are chosen as $k_1 = -1$ and $k_2 = 0.018$. This section, aims to verify that the iPOD can improve the attenuation of power oscillations in the system under contingencies given a random operating point (see Section III-C1), and compare it to the conventional PSS performance in the well-known two area system used as a reference [21].

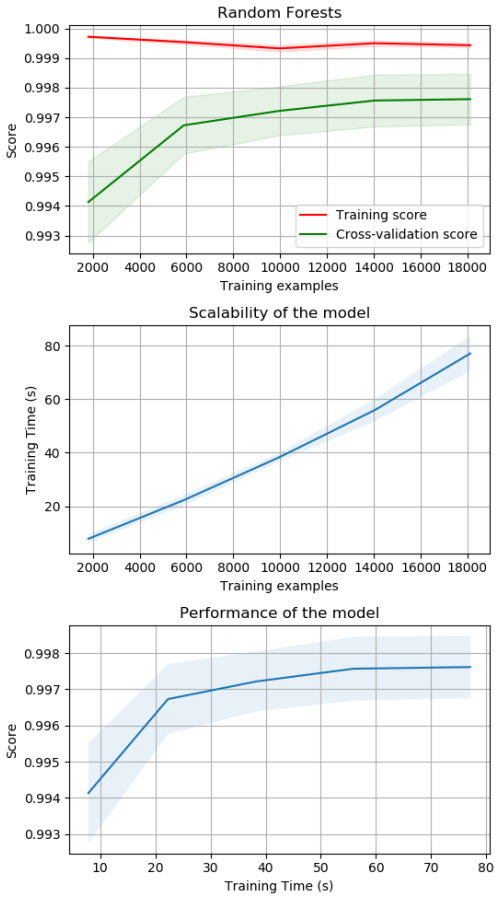

FIGURE 10. Learning curves on $\Im\{\lambda\}$ component.

A. SYSTEM RESPONSE TO DISTURBANCE

To excite the inter-area mode a 3-phase fault is defined in the middle of the upper transmission line that connects bus 7 and 8 i.e. L^1_{7-8}. The fault is cleared by opening the breakers at both ends and re-closing them after 100ms. As mentioned, loads in areas 1 and 2 are set randomly to move the system at a new operating point. The snapshot of the system at time t_m (before fault occurrence) is fed into RF, which makes a prediction about the inter-area to tune the SPC.

Note that in this study communication delays have not been considered, hence all measurements at t_m are in sync. In reality, however, this might not be the case. Typically, a data storing and preprocessing module handles the information flow before they are passed on for further processing [28].Communication protocols, such as the well known IEC 61850, which support timestamping are used for ensuring that measurements can be sorted according to their corresponding time tags [29], [30].

Illustrated in Fig. 12 is the frequency recorded at buses 6 and 10 of areas 1 and 2, respectively. As a comparison the

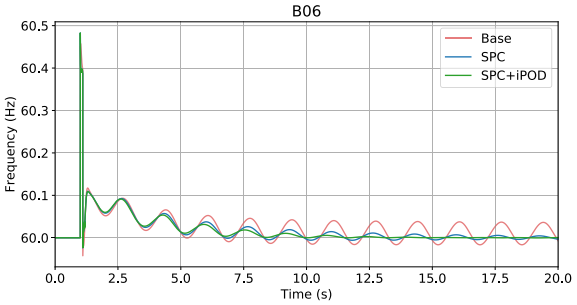

FIGURE 11. Frequency response in area 1 for a random operating point and a 3-phase fault in L^1_{7-8}.

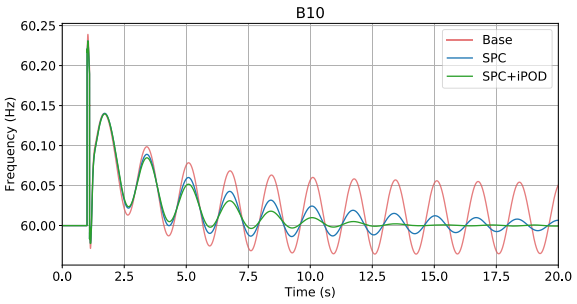

FIGURE 12. Frequency response in area 2 for a random operating point and a 3-phase fault in L^1_{7-8}.

system response with the proposed SPC equipped with the iPOD is plotted against the base case (i.e. without SPC) and the SPC-only case (i.e. without online tuning and attenuation of low-frequency power oscillations).

The inherent capability of the regular SPC to damp oscillations is revealed in the frequency response of both areas [31]. Yet, by predicting the mode frequency and re-tune the iPOD parameters the damping can be enhanced even further when the SPC+iPOD is used, as it is shown in Fig. 12, forcing oscillations to decay faster.

Concretely, the stochastic variations of loads cause the inter-area mode to vary in both frequency and damping, therefore, it is vital to be able to monitor these changes. The SPC can significantly improve damping of inter-area modes as shown in Fig. 13 depicting the results of modal analysis for random operating points. It is worth noting that the effectiveness of the iPOD scheme reflects the accuracy of the RF predictions.

B. OSCILLATION DAMPING IMPACT OF iPOD TO SYNCHRONOUS GENERATORS

In the two area system, the load L09 in area 2 is approximately 1.5 times larger than L07 of area 1. As a consequence, area 2 relies on imported power to maintain power balance. The power dependence of area 2 can be seen by analysing the power oscillations in each generator. Specifically, these responses during the symmetrical fault in L^1_{7-8} for a random operating point are depicted in Fig. 14 for area 1 and in Fig. 15 for area 2.

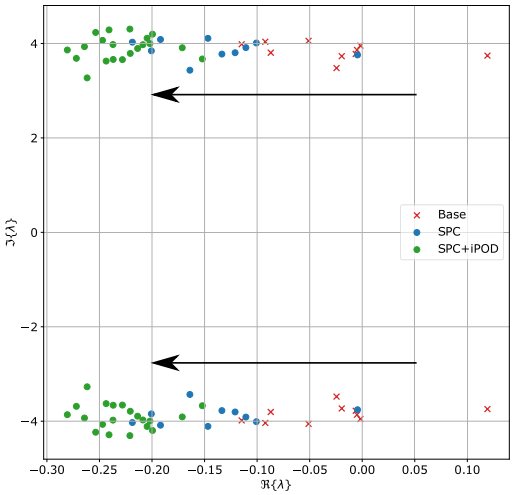

FIGURE 13. Modal analysis for random operating points.

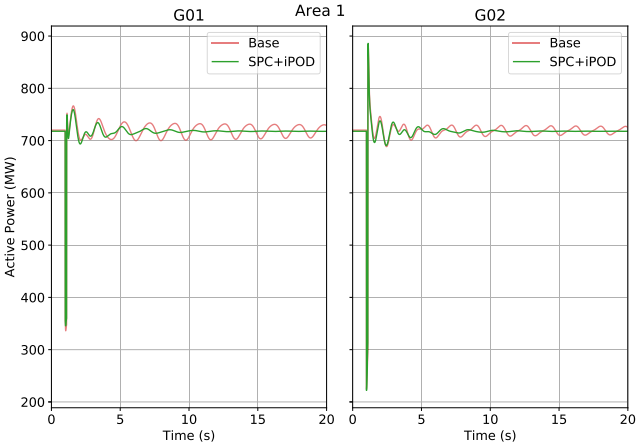

FIGURE 14. Instantaneous active power of generators in area 1 for a random operating point and a 3phase fault in L^1_{7-8}.

TABLE 4. On-fault instantaneous peak power output (in MW).

		G01	G02	G03	G04
Base	Max	752.26	884.06	774.94	760.49
	Min	336.22	225.17	628.32	571.44
SPC+iPOD	Max	749.32	886.00	747.56	759.19
	Min	345.54	222.04	615.92	586.84

As expected, the generators in area 2 are oscillating with higher amplitudes than those in area 1. Inter-area modes can result in power fluctuations, which can stress the structural integrity of generator units. By integrating the iPOD in the conventional SPC, the system power oscillations decay at a higher rate reducing the stress on generator shafts. This becomes even more obvious in area 2 where a 100MW oscillation can damage generators 3 and 4. Furthermore, the output power excursions during the on-fault period are reduced for all generators but generator 2, where there exists a slight increase of peak power as listed in Table 4. Nevertheless, it is

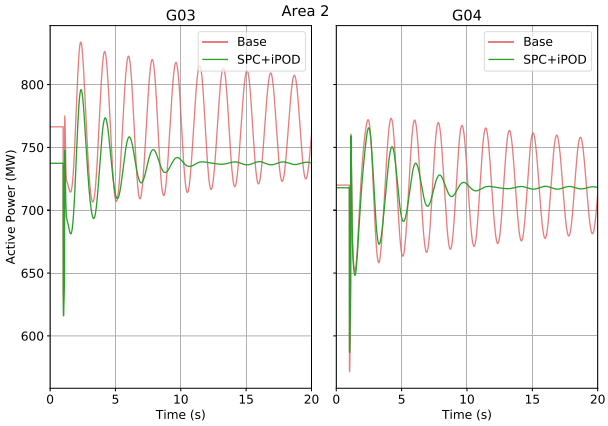

FIGURE 15. Instantaneous active power of generators in area 2 for a random operating point and a 3phase fault in L_{7-8}^{1}.

TABLE 5. Parameters of PSS.

Plant	G1	G2	G3	G4
K	37.154	14.704	26.665	33.268
T1	2.0989	1.1687	2.8100	0.6577
T2	0.2499	1.4871	2.6542	1.7089
T3	0.8846	0.7328	2.9059	1.7834
T4	0.6693	2.5904	0.2257	0.8669
Tw	10.	10.	10.	10.
y_{min}	-0.2	-0.2	-0.2	-0.2
y_{max}	0.2	0.2	0.2	0.2

TABLE 6. Averaged modal analysis results per control scenario.

Controller	Freq. (Hz)	Damp.	Damp. Ratio
Base	0.613	0.019	0.50%
PSS1	0.604	0.289	7.60%
PSS2	0.614	0.022	0.58%
PSS3	0.582	0.359	9.79%
PSS4	0.617	0.061	1.59%
SPC+iPOD	0.659	0.229	5.55%

worth emphasizing that the improved damping from the SPC based on iPOD is achieved with only 1/7 of the synchronous generator apparent power.

C. iPOD COMPARISON WITH PSS

Commonly, the PSS is used to provide damping of critical modes in a system. This section compares the individual contribution of each PSS device with the corresponding contribution provided by the SPC augmented by the iPOD. For the purpose of this study, the PSS parameters are considered fixed and their values are set following the methodology described in [32] and listed in Table 5. Concretely, random points are generated following the aforementioned process and for each control scenario modal analysis of the system is performed. The results, averaged over all random points, are listed in Table 6.

Clearly, PSS1 and PSS3, on average, possess the highest contribution towards inter-area power oscillation damping. However, damping provided by PSS1 and PSS3 varies significantly between each case. Particularly, PSS1 fails to provide damping for the inter-area mode for a random operating as

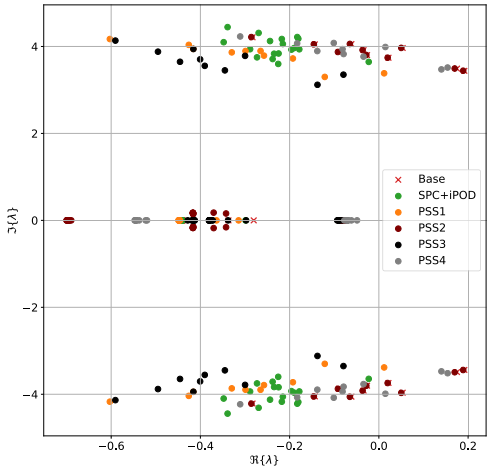

FIGURE 16. Eigenvalues of system per control scenario.

revealed in Fig. 16. As opposed, the SPC augmented by iPOD seems to provide less damping than the previous two PSS devices. However, as Fig. 16 shows, this amount does not fluctuate much highlighting the damping capabilities of the SPC with iPOD. Furthermore, it also dominates over the contribution of both PSS2 and PSS4, which due to poor tuning are unable to damp the inter-area mode corresponding to the random operating points. Note that the nominal power of the SPC is considerably lower to the nominal power of the synchronous generators.

V. CONCLUSION

The connection of energy systems through power electronic devices is adding to the complexity of power systems by altering the overall behaviour of power systems. Rotor angle stability is of primary concern as the presence of power electronics in power systems is rising. Conventional PSS are performing acceptably for attenuating oscillatory modes, however, only for a narrow range of operating conditions. Power converters controlled through grid-forming techniques, e.g. a SPC augmented by an iPOD as in this paper, can provide an additional source for damping power oscillations with the use of data and AI.

Random Forest is a powerful machine learning model, which exploit the inherent diversity of combing individual decisions trees trained with random subsets of the original dataset. In this paper, two random forests have been developed for predicting the real and imaginary component of the inter-area mode in the two are system. These predictions are used to tune the iPOD added to SPC for improving damping of the targeted inter-area mode. As it has been proven from thorough analyses, the SPC with iPOD can enhance the stability of a power system by increasing the damping of the inter-area mode. In the test presented in this paper, the response of recorded frequency demonstrated significant improvement when SPC is augmented by the iPOD scheme. In contrast to conventional PSS, the iPOD does not have a phase lag and

only the frequency of the oscillation is required. Therefore, reducing the number of parameters needed to be tuned for attenuating the inter-area mode.

Furthermore, the proposed scheme is shown to be robust against network variations, performing equally and even better than the conventional PSS in the system. However, the proposed control scheme should not be considered as an adversary of PSS but rather as a complementary ally for improving the performance of the power systems of the future, which will be dominated by power electronics. The increased utilization of grid-forming converters for additional functionalities other than their primary purpose will increase flexibility and robustness in the ever-changing power system environment without the necessity for additional investments.

ACKNOWLEDGMENTS

This work was supported in part by the European Commission under Project FLEXITRANSTORE—H2020-LCE-2016-2017-SGS-774407, and in part by the Spanish Ministry of Science under Project ENE2017-88889-C2-1-R. Any opinions, findings and conclusions or recommendations expressed in this material are those of the authors and do not necessarily reflect those of the host institutions or funders.

REFERENCES

[1] L. Meegahapola and D. Flynn, "Impact on transient and frequency stability for a power system at very high wind penetration," in *Proc. IEEE PES Gen. Meeting*, Jul. 2010, pp. 1–8.

[2] *High Penetration of Power Electronic Interfaced Power Sources (HPoPEIPS) ENTSO-E Guidance Document for National Implementation for Network Codes on Grid Connection*, ENTSO-E, Brussels, Belgium, 2017.

[3] Z. A. Obaid, L. M. Cipcigan, and M. T. Muhssin, "Power system oscillations and control: Classifications and PSSs' design methods: A review," *Renew. Sustain. Energy Rev.*, vol. 79, pp. 839–849, Nov. 2017. [Online]. Available: http://www.sciencedirect.com/science/article/pii/S1364032117307499

[4] I. Kamwa, R. Grondin, and G. Trudel, "IEEE PSS2B versus PSS4B: The limits of performance of modern power system stabilizers," *IEEE Trans. Power Syst.*, vol. 20, no. 2, pp. 903–915, May 2005.

[5] *IEEE Recommended Practice for Excitation System Models for Power System Stability Studies*, IEEE Standard 421.5-2016 (Revision IEEE Std 421.5-2005), Aug. 2016, pp. 1–207.

[6] F. Rashidi and M. Rashidi, "Robust and adaptive tuning of power system stabilizers using artificial neural networks," in *Innovations in Applied Artificial Intelligence*. Berlin, Germany: Springer, Jul. 2004, pp. 1023–1032.

[7] J. Fang, H. Li, Y. Tang, and F. Blaabjerg, "On the inertia of future more-electronics power systems," *IEEE J. Emerg. Sel. Topics Power Electron.*, vol. 7, no. 4, pp. 2130–2146, Dec. 2019.

[8] W. Zhang, A. Tarraso, J. Rocabert, A. Luna, J. I. Candela, and P. Rodriguez, "Frequency support properties of the synchronous power control for grid-connected converters," *IEEE Trans. Ind. Appl.*, vol. 55, no. 5, pp. 5178–5189, Sep. 2019.

[9] J. Rocabert, A. Luna, F. Blaabjerg, and P. Rodríguez, "Control of power converters in AC microgrids," *IEEE Trans. Power Electron.*, vol. 27, no. 11, pp. 4734–4749, Nov. 2012.

[10] S. Yazdani, M. Ferdowsi, M. Davari, and P. Shamsi, "Advanced current-limiting and power-sharing control in a PV-based grid-forming inverter under unbalanced grid conditions," *IEEE J. Emerg. Sel. Topics Power Electron.*, vol. 8, no. 2, pp. 1084–1096, Jun. 2020.

[11] A. Tayyebi, D. Groß, A. Anta, F. Kupzog, and F. Dörfler, "Frequency stability of synchronous machines and grid-forming power converters," *IEEE J. Emerg. Sel. Topics Power Electron.*, vol. 8, no. 2, pp. 1004–1018, Jun. 2020.

[12] M. G. Taul, X. Wang, P. Davari, and F. Blaabjerg, "Current limiting control with enhanced dynamics of grid-forming converters during fault conditions," *IEEE J. Emerg. Sel. Topics Power Electron.*, vol. 8, no. 2, pp. 1062–1073, Jun. 2020.

[13] P. Rodriguez, C. Citro, J. I. Candela, J. Rocabert, and A. Luna, "Flexible grid connection and islanding of SPC-based PV power converters," *IEEE Trans. Ind. Appl.*, vol. 54, no. 3, pp. 2690–2702, May 2018.

[14] A. Tarraso, N.-B. Lai, G. N. Baltas, and P. Rodriguez, "Power quality services provided by virtually synchronous FACTS," *Energies*, vol. 12, no. 17, p. 3292, 2019. [Online]. Available: https://www.mdpi.com/1996-1073/12/17/3292

[15] P. R. Cortes, J. I. C. Garcia, J. R. Delgador, and R. Teodorescu, "Virtual controller of electromechanical characteristics for static power converters," Europen Patent 2 683 075 A1, Jan. 8, 2014.

[16] M. Pérez-Ortiz, S. Jiménez-Fernández, P. Gutiérrez, E. Alexandre, C. Hervás-Martínez, and S. Salcedo-Sanz, "A review of classification problems and algorithms in renewable energy applications," *Energies*, vol. 9, no. 8, p. 607, 2016. [Online]. Available: https://www.mdpi.com/1996-1073/9/8/607

[17] G. N. Baltas, C. Perales-González, P. Mazidi, F. Fernandez, and P. Rodriguez, "A novel ensemble approach for solving the transient stability classification problem," in *Proc. 7th Int. Conf. Renew. Energy Res. Appl. (ICRERA)*, Oct. 2018, pp. 1282–1286.

[18] J. J. Q. Yu, D. J. Hill, A. Y. S. Lam, J. Gu, and V. O. K. Li, "Intelligent time-adaptive transient stability assessment system," *IEEE Trans. Power Syst.*, vol. 33, no. 1, pp. 1049–1058, Jan. 2018.

[19] P. McNabb, D. Wilson, and J. Bialek, "Classification of mode damping and amplitude in power systems using synchrophasor measurements and classification trees," *IEEE Trans. Power Syst.*, vol. 28, no. 2, pp. 1988–1996, May 2013.

[20] F. Sulla, E. Måsbäck, and O. Samuelsson, "Linking damping of electromechanical oscillations to system operating conditions using neural networks," in *Proc. IEEE PES Innov. Smart Grid Technol., Eur.*, Oct. 2014, pp. 1–6.

[21] P. Kundur, N. J. Balu, and M. G. Lauby, *Power System Stability and Control* (The Epri Power System Engineering). New York, NY, USA: McGraw-Hill, 1994.

[22] R. Badar and J. Shair, "Adaptive NeuroFuzzy sliding mode based damping control for SSSC," in *Proc. SAI Intell. Syst. Conf. (IntelliSys)*, Y. Bi, S. Kapoor, and R. Bhatia, Eds. Cham, Switzerland: Springer, 2018, pp. 91–106.

[23] R. O. Duda, P. E. Hart, and D. G. Stork, *Pattern Classification*, 2nd ed. Hoboken, NJ, USA: Wiley, 2001.

[24] S. Theodoridis and K. Koutroumbas, *Pattern Recognition*, 4th ed. New York, NY, USA: Academic, 2008.

[25] L. Breiman, "Random forests," *Mach. Learn.*, vol. 45, no. 1, pp. 5–32, Oct. 2001, doi: 10.1023/A:1010933404324.

[26] S. Shalev-Shwartz and S. Ben-David, *Understanding Machine Learning: From Theory to Algorithms*. Cambridge, U.K.: Cambridge Univ. Press, 2014.

[27] F. Pedregosa, G. Varoquaux, A. Gramfort, V. Michel, B. Thirion, O. Grisel, M. Blondel, P. Prettenhofer, R. Weiss, V. Dubourg, J. Vanderplas, A. Passos, D. Cournapeau, M. Brucher, M. Perrot, and E. Duchesnay, "Scikit-learn: Machine learning in Python," *J. Mach. Learn. Res.*, vol. 12, pp. 2825–2830, Nov. 2011.

[28] K. Diakos, Q. Wu, and A. H. Nielsen, "Phasor measurement unit and phasor data concentrator test with real time digital simulator," in *Proc. IEEE PES Asia–Pacific Power Energy Eng. Conf. (APPEEC)*, Dec. 2014, pp. 1–5.

[29] T. S. Ustun, S. M. Farooq, and S. M. S. Hussain, "A novel approach for mitigation of replay and masquerade attacks in smartgrids using IEC 61850 standard," *IEEE Access*, vol. 7, pp. 156044–156053, 2019.

[30] T. S. Ustun, S. M. Farooq, and S. M. S. Hussain, "Implementing secure routable GOOSE and SV messages based on IEC 61850-90-5," *IEEE Access*, vol. 8, pp. 26162–26171, 2020.

[31] M. Abdollahi, J. I. Candela, J. Rocabert, M. A. Elsaharty, and P. Rodriguez, "Novel analytical method for dynamic design of renewable SSG SPC unit to mitigate low-frequency electromechanical oscillations," *IEEE Trans. Power Electron.*, vol. 35, no. 7, pp. 7532–7544, Jul. 2020.

[32] A. Stativă and F. Gonzalez-Longatt, "Peer-to-peer (P2P) MATLAB–PowerFactory communication: Optimal placement and setting of power system stabilizer," in *Advanced Smart Grid Functionalities Based on PowerFactory*. Cham, Switzerland: Springer, 2018, pp. 301–318, doi: 10.1007/978-3-319-50532-9_12.

GREGORY N. BALTAS (Student Member, IEEE) received the B.S. degree in electrical engineering from the Technological Educational Institute of Central Greece, Chalkis, Greece, in 2015, and the M.S. degree in power engineering from the University of Sydney, Sydney, Australia. He is currently pursuing the Ph.D. degree in data science with the Universidad Loyola Andalucía,

Since 2018, he has been a Research Assistant with the Loyola Institute of Science and Technology (Loyola.TECH), Universidad Loyola Andalucía. His research interests include applied artificial intelligence, power system stability, and autonomous energy systems.

NGOC BAO LAI (Student Member, IEEE) received the B.S. degree in electrical engineering from the Danang University of Science and Technology, Da Nang, Vietnam, in 2014, and the M.S. degree in electrical and information engineering from the Seoul National University of Science and Technology, Seoul, South Korea, in 2017. He is currently pursuing the Ph.D. degree in electrical engineering wtih the Universitat Politècnica de Catalunya (UPC).

Since 2018, he has been a Research Assistant with Universidad Loyola Andalucía. His research interests include robust control, power electronics, and distributed generation systems.

LEONARDO MARIN (Student Member, IEEE) received the B.S. degree in industrial engineering from Cuenca University, Cuenca, Ecuador, in 2005, and the M.S. degree in automatic systems and industrial electronics engineering from the Polytechnic University of Catalonia (UPC), Barcelona, Spain, in 2015. He is currently pursuing the Ph.D. degree in electrical engineering with the Renewable Electrical Energy System Research Centre, Universitat Politècnica de Catalunya (UPC). Since 2019, he has been a Research Assistant with Universidad Loyola Andalucía. His research interests include the dynamic and stability analyses of power systems with high-penetration of renewable energies, HVDC and hybrid systems, distributed generation systems, and microgrids.

ANDRÉS TARRASÓ (Student Member, IEEE) received the M.Sc. degree in electrical engineering from the Technical University of Catalonia, Barcelona, Spain, in 2017. He is currently pursuing the Ph.D. degree with the Technical University of Catalonia, Barcelona. From 2017, he has been a Research Assistant with the Department of Electrical Engineering, Technical University of Catalonia, where he has been a Researcher and an Assistant Professor with the Department of Electrical Engineering. His current research interests include power electronics, photovoltaics, wind energy systems, and microgrids.

PEDRO RODRIGUEZ (Fellow, IEEE) received the M.Sc. and Ph.D. degrees in electrical engineering from the Technical University of Catalonia (UPC), Spain, from 1994 and 2004, respectively. He was a Postdoctoral Researcher with CPES, Virginia Tech, USA, the Department of Energy Technology, Aalborg University (AAU), Denmark, and the MIT Energy Initiative (MITie), Boston, USA. He was a Co-Supervisor of the Vestas Power Program, Denmark, from 2007 to 2011. He was a Director of the technology on modern power systems at Abengoa Research, from 2011 to 2017. Since 2017, he has been a Full Professor with the Loyola University Andalucia, where he is the Head of LOYOLA.Tech, leading a Research Program on Intelligent Energy Systems. He is also linked with the UPC as a part-time Professor. He is in the Clarivate's list of Highly Cited Researchers in Engineering, from 2015 to 2018. He has coauthored one Wiley-IEEE book, more than 100 articles in ISI technical journals, and around 300 articles in conference proceedings. He is the holder of 16 licensed patents. He has participated in more than 50 projects with industrial partners and several EU projects. He is a IEEE Fellow for his contributions in the control of distributed generation. He has served as an Associate Editor of the IEEE TRANSACTION ON POWER ELECTRONICS, the IEEE JOURNAL ON EMERGING AND SELECTED TOPICS ON POWER ELECTRONICS, the IEEE JOURNAL ON INDUSTRIAL ELECTRONICS AND ENERGIES. His research interests include intelligent energy systems, distributed generation, and universal energy access.